# Long-range ferromagnetic order in LaCoO_{3−δ} epitaxial films due to the interplay of epitaxial strain and oxygen vacancy ordering

V. V. Mehta, N. Biskup, C. Jenkins, E. Arenholz, M. Varela, and Y. Suzuki

# Long Range Ferromagnetic Order in LaCoO$_{3-\delta}$: the Role of Epitaxial Strain and Oxygen Vacancies

V. V. Mehta*,[1, 2] N. Biskup,[3, 4] C. Jenkins,[5] E. Arenholz,[5] M. Varela,[3, 4] and Y. Suzuki[1, 2, 6, 7]

[1]*Dept. of Materials Science and Engineering, University of California, Berkeley, CA 94720, USA*
[2]*Materials Sciences Division, Lawrence Berkeley National Laboratory, Berkeley, CA 94720, USA*
[3]*Departamento de Fisica Aplicada III, Universidad Complutense de Madrid, Spain*
[4]*Materials Science and Technology Division, Oak Ridge National Laboratory*
[5]*Advanced Light Source, Lawrence Berkeley National Laboratory, Berkeley, CA 94720, USA*
[6]*Geballe Laboratory for Advanced Materials, Stanford University, Stanford, CA 94305, USA*
[7]*Department of Applied Physics, Stanford University, Stanford, CA 94305, USA*
(Dated: March 31, 2015)

We demonstrate that a combination of electronic structure modification and oxygen vacancy ordering can stabilize a long range ferromagnetic ground state in epitaxial LaCoO$_3$ thin films. Highest saturation magnetization values are found in the thin films in tension on SrTiO$_3$ and (La,Sr)(Al,Ta)O$_3$ substrates and the lowest values found in thin films in compression on LaAlO$_3$. Electron microscopy reveals oxygen vacancy ordering to varying degrees in all samples although samples with the highest magnetization are the most defective. Element-specific X-ray absorption techniques reveal the presence of high spin Co$^{2+}$ and possibly Co$^{3+}$ as well as low spin Co$^{3+}$ in different proportions depending on the strain state. The interactions among the high spin Co ions and the oxygen vacancy superstructure are correlated with the stabilization of the long-range ferromagnetic order.

The ground state of materials close to a phase transition- be it a metal-insulator, magnetic transition etc.- may be modified by external parameters to stabilize a state on the other side of this phase transition. There have been numerous studies utilizing electric or magnetic fields and strain to generate such effects. However the generation of long-range order in thin film form, not observed at any measureable temperature in the bulk, is unexpected. A particularly surprising example is the observation of ferromagnetism in epitaxial thin films of nominally undoped LaCoO$_3$ (LCO). In the bulk, the compound exhibits a diamagnetic, low spin (LS) state at low temperatures with a transformation to a paramagnetic high or intermediate spin (HS or IS) state at higher temperatures marked by a spin state transition. Early bulk work suggests long range magnetic ordering of LS and HS Co ions[1] while more recent bulk work appears to exhibit surface ferromagnetism.[2] In epitaxial films, the origin of this long range magnetic order has been attributed to the stabilization of HS Co ions via epitaxial strain accompanied by a superexchange interaction among HS Co$^{3+}$ and LS Co$^{3+}$ ions[3] or among HS Co$^{2+}$ and LS Co$^{3+}$ ions.[4] However epitaxial strain alone cannot explain the observation of long-range ferromagnetic order in some epitaxial films[5–7] and not in others.[8–10]

The role of defects must also be taken into consideration as it has been shown that oxygen stoichiometry can significantly affect the functional properties of the sys-

tem. For example, while stoichiometric LaMnO$_3$ is an antiferromagnetic insulator, experimentally samples tend to be oxygen deficient and exhibit ferromagnetism.[11] The antiferromagnetic insulator LuMnO$_3$ has also been found to stabilize a ferromagnetic ground state when grown in epitaxial thin film form. In this case, the ferromagnetism is found close to the film substrate interface where strain effects are largest.[12] More recent studies of epitaxial (La,Sr)CoO$_3$ (LSCO) films on similarly lattice-matched NdGaO$_3$ and (La,Sr)(Al,Ta)O$_3$ (LSAT) substrates showed different saturation magnetization values.[13] In these studies, the authors demonstrate that the different oxygen vacancy content of the films grown on the two different substrates can account for the enhancement of the magnetic properties. While some[9,10] have cited chemical inhomogeneity as the cause of the long-range ferromagnetic order in epitaxial LCO films, an explanation of how these defects could be responsible for the stabilization of a long-range ferromagnetic ground state is still lacking. Recent work has presented the possibility of added complexity due to the possibility of ferroelastic behavior coupling to the strain dependent magnetism in these films.[14] However, some of our recent work suggests that ordered oxygen vacancies may also account for the generation of long-range ferromagnetic order via the stabilization of ordered high spin Co$^{2+}$ cations.[4]

We have undertaken a systematic study of the combined effects of epitaxial strain and defects on the magnetism in epitaxial LCO thin films. Our study indicates that both factors affect the magnetic response and are interrelated as the epitaxial strain induces the formation of oxygen vacancy ordering in particular directions. Through a comparative study of epitaxial LCO thin films

*currently at HGST, A Western Digital Company, San Jose Research Center, San Jose, CA, 95135

grown on SrTiO$_3$ (STO), LSAT and LaAlO$_3$ (LAO) substrates, we find that the stabilization of higher spin Co$^{2+}$ and possibly Co$^{3+}$ states combined with an ordered oxygen vacancy superstructure can account for a ferromagnetic exchange interaction observed in many but not all of our LCO thin films. We perform detailed structural characterization of the strain state of our samples using reciprocal space mapping in X-ray diffraction. Scanning transmission electron microscopy and electron energy loss spectroscopy studies reveal oxygen vacancy ordering in our samples to varying degrees. We correlate these structural and vacancy ordering variations with the electronic structure and magnetism. Element specific X-ray absorption spectroscopy (XAS) indicates that there are HS Co$^{2+}$, LS Co$^{3+}$, and possibly HS Co$^{3+}$ ions in the epitaxial films. SQUID magnetometry reveals ferromagnetic order primarily in the epitaxial LCO films under tensile strain. Element specific X-ray magnetic circular dichroism indicates that the long-range ferromagnetic order originates from HS Co$^{2+}$ ions and possibly HS Co$^{3+}$ ions. By exploring the relationship between magnetism, strain, and stoichiometry in detail using microstructure and electronic structure characterization, we experimentally uncover the crucial factors needed to explain the long-range magnetic order in epitaxial LCO thin films.

## I. EXPERIMENT

LCO films were grown on STO, LSAT, and LAO substrates in a large range of thicknesses (8 nm - 133 nm thick) using pulsed-laser deposition with a 248 nm KrF laser ($\sim$1 J/cm$^2$) pulsed at 3 Hz. Films grown on STO (mismatch = a$_{substrate}$-a$_{LCO}$/a$_{LCO}$ $\sim$2.6%) and LSAT (1.5%) are under in-plane tensile strain and films on LAO (-0.8%) are under in-plane compressive strain. The films were grown at 700°C in 320 mTorr of O$_2$ and cooled in an atmosphere of 1 Torr of O$_2$. Film thicknesses were determined using X-ray reflectivity, and the structure of the films was determined by X-ray diffraction (XRD). Rutherford backscattering spectroscopy (RBS) indicates that all films have a one to one La:Co ratio to within the accuracy of the RBS measurement. 15 nm and 75 nm thick samples on LAO, LSAT, and STO substrates were measured at Oak Ridge National Laboratory using high resolution Scanning Transmission Electron Microscopy (STEM) and Electron Energy Loss Spectroscopy (EELS) to obtain detailed local structural and chemical information. X-ray absorption (XA) and X-ray linear dichroism (XLD) measurements were performed at the Advanced Light Source to probe the films' electronic structure when grown on these substrates with different thicknesses. A superconducting quantum interference device (SQUID) magnetometer was used to determine bulk magnetic response of the films, and X-ray magnetic circular dichroism (XMCD) measurements were used to obtain element specific magnetic information.

## II. STRUCTURE

### A. X-ray Diffraction

Investigation of the structure of LCO films on STO, LSAT, and LAO substrates reveals coherently strained thin films as well as partially-relaxed thicker films under both tensile and compressive strain due to the substrate-film lattice mismatch. Detailed studies of the films' microstructure using STEM and EELS reveal that the magnitude and pattern of oxygen-related defects are also related to the strain state in the film.

The films' structure measured by XRD reveals information regarding both the crystallinity and the in-plane (IP) and out-of-plane (OOP) lattice parameters as a function of the substrate-film lattice mismatch. The crystalline quality was assessed by $\Delta\omega$ measured at full-width half maximum (FWHM) from $\omega$ rocking curve measurements in 8 nm - 133 nm thick films. In general, the crystalline quality decreases with increasing film thickness. Films show good crystallinity below 50 nm thick with $\Delta\omega$ ranging from 0.12°-0.32°. At larger thicknesses the mosaic spread increases considerably to $\Delta\omega > 0.5°$, due to an increase in defects associated with structural relaxation.

The $\theta-2\theta$ XRD measurements of the 002 peak (Figure 1) reveal that the structure evolves toward a relaxed bulk-like LCO structure as a function of increasing thickness. The $2\theta$ values (and lattice parameters) in the figure were obtained after fitting a Gaussian distribution to the film peaks and using the Gaussian peak position. Films less than 15 nm thick show OOP lattice parameters significantly changed relative to the bulk value of $\sim$3.81 Å. Films on LAO (Figure 1(a)) show a larger OOP lattice parameter $\sim$3.85 Å while films on LSAT (Figure 1(b)) and STO (Figure 1(c)) have OOP lattice parameters depressed with respect to bulk LCO with values of $\sim$3.80 Å and $\sim$3.77 Å respectively. Thicker films on LAO and STO show OOP lattice parameters that clearly relax toward bulk LCO. Intriguingly, OOP peaks for thick films on LSAT do not show any significant shift in $2\theta$ but broaden and increase in intensity with increasing thickness, suggesting that even at these larger thicknesses a significant portion of the film remains coherently strained.

To understand better the overall structural changes as a function of thickness on the different substrates, we compared reciprocal space maps (RSMs) taken at the 013 peak for $\sim$15 nm and $\sim$95 nm thick films (Figure 2). The thinner films on all three substrates are coherently strained to the underlying substrates and exhibit modified lattice parameters consistent with the $\theta-2\theta$ measurements in Figure 1. The thick films show different degrees of partial relaxation of the film peak towards bulk LCO values. This partial relaxation suggests that the appearance of a constant OOP lattice parameter for a range of LCO thickness on LSAT, as deduced from $\theta-2\theta$ measurements, is misleading. LSAT films are in fact re-
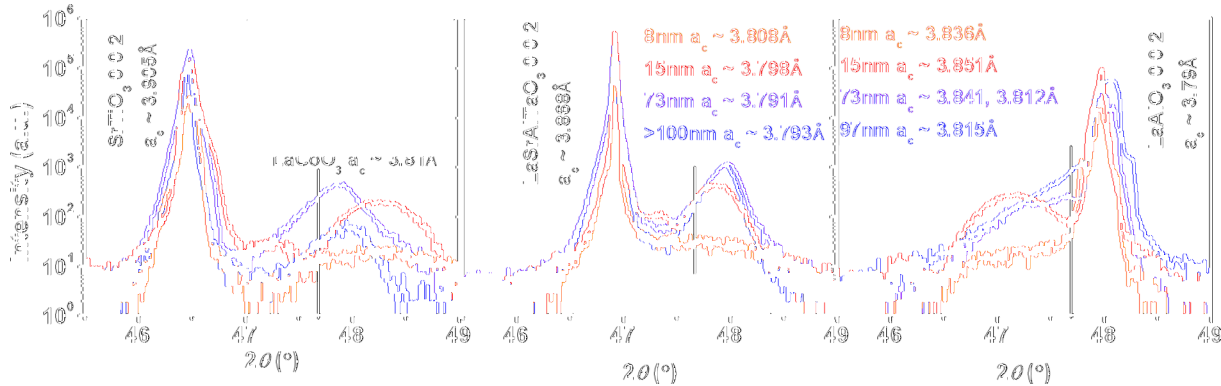
FIG. 1: (color online) $\theta-2\theta$ measurements around 002 peak showing evolution of OOP lattice parameter as a function of thickness on (a) STO, (b) LSAT, and (c) LAO substrates respectively.

laxing, though to a lesser degree compared to STO and LAO films. In addition, all thick films show a severely broadened peak indicative of larger mosaic spread, consistent with our OOP $\omega$ scans. These results suggest the presence of strain gradients in these thick films.

Coherently strained LCO films less than 15 nm thick indicate tetragonally distorted unit cells for LCO on each substrate. Table I lists average value for IP and OOP lattice parameters (determined from RSMs) for three sets of coherently strained films grown less than 15 nm thick. We typically achieve c/a $\sim$1.015 with coherently strained films in compression on LAO, and c/a $\sim$0.979 and c/a $\sim$0.965 for the comparably thin films strained in tension on LSAT and LAO. As thickness is increased, the LCO films on all substrates evolve from a tetragonally distorted lattice toward a cubic one approaching c/a $\sim$1. These lattice distortions in the coherently strained films can be decomposed into volume preserving and non-volume preserving contributions to the strain. The two contributions are deduced from $2\varepsilon_{zz}$ - $\varepsilon_{xx}$ - $\varepsilon_{yy}$ (which describes a volume conserving tetragonal distortion) and $\varepsilon_{xx}$ + $\varepsilon_{yy}$ + $\varepsilon_{zz}$ (which describes volume changing distortion). For these calculations we have assumed that the bulk LCO unit cell volume $\sim$55.306 Å$^3$ and that $\varepsilon_{xx}$ = $\varepsilon_{yy}$, since the films are grown on 001 substrates with approximately cubic symmetry. We find that films on LSAT and STO show significant tetragonal distortion as well as volume change. Films compressively strained on LAO only show a change in the tetragonal distortion with little volume change. The ratio of the volume change to tetragonal distortion (last column in Table I) provides an indication of the different modes by which strain is accommodated in films on the different substrates.

### B. Scanning Transmission Electron Microscopy

XRD provides a measure of the *average* lattice parameters for LCO under different degrees of epitaxial strain. In order to probe the local structure, we used

STEM, which revealed that the epitaxial strain is accommodated through structurally ordered changes in oxygen stoichiometry[15] (Figure 3). $CoO_2$ planes, exhibiting a signficantly darker contrast, were found in 15 nm thick samples on LAO, LSAT, and STO. These dark stripes appeared perpendicular to the substrate-film interface in films on LSAT (Figure 3(b)) and STO (Figure 3(c)) and parallel to this interface in films on LAO (Figure 3(a)). The dark Co-O planes occur periodically every 3(sometimes 4) perovskite blocks on STO and LAO, and after every 2-3 unit cells on LSAT. Similar dark contrast Co-O planes have been observed in other Sr-doped cobaltite films and have been associated with oxygen vacancies,[15–18] cation vacancies,[19] and even ferroelastic structural twinning.[20,21] More recently, Choi *et al.* found similar dark contrast planes and attributed them to a ferroelastic mechanism associated with epitaxial strain.[14]

Figure 3(d, e, f) show the O-K EELS edges extracted from line scans acquired along the dark stripes (black line) and bright planes (red line) of $CoO_2$. The spectral differences between both types of Co-O planes are easily discernible in films on LAO and STO. In general, the bright perovksite blocks have higher O K-edge intensities with an obvious shoulder peak at $\sim$527 eV, pointing to a higher local O concentration along these planes. The dark stripes have a higher $L_3/L_2$ peak intensity ratio at the Co-L edges (Figure 3(g, h, i)), revealing reduced Co atoms.[4] These spectral differences between bright and

TABLE I: Average structural values determined from X-ray diffraction reciprocal space maps for three different sets of films <15 nm thick. Only the IP and OOP values are experimentally determined.

| Substrate (001) | IP (Å) | OOP (Å) | c/a | V (Å$^3$) | $\Delta$V or $\varepsilon_{xx}$+$\varepsilon_{yy}$+$\varepsilon_{zz}$ (%) | $2\varepsilon_{zz}$-$\varepsilon_{xx}$-$\varepsilon_{yy}$ (%) | $\varepsilon_{xx}$+$\varepsilon_{yy}$+$\varepsilon_{zz}$(%)/ $2\varepsilon_{zz}$-$\varepsilon_{xx}$-$\varepsilon_{yy}$(%) |
|---|---|---|---|---|---|---|---|
| STO | 3.90 | 3.767 | 0.965 | 57.256 | 3.53 | -7.02 | -0.503 |
| LSAT | 3.87 | 3.790 | 0.979 | 56.802 | 2.70 | -4.27 | -0.632 |
| LAO | 3.79 | 3.845 | 1.015 | 55.242 | -0.11 | 2.93 | -0.023 |
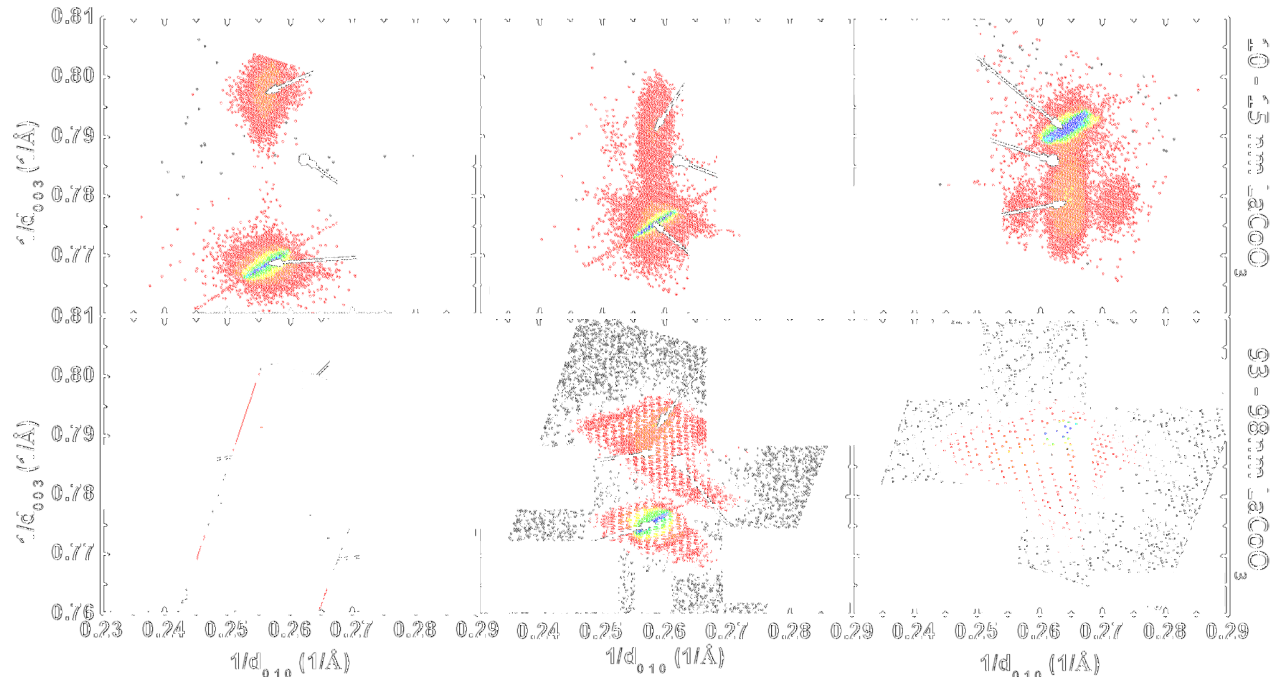
FIG. 2: (color online) Reciprocal space maps showing 013 peak reflections for the ∼15 nm (a,b,c) and ∼95 nm (d,e,f) LCO films grown on STO (a,d), LSAT (b,e), and LAO (c,f).

dark contrast planes indicate that the dark stripes are oxygen deficient atomic planes as previous works have reported. The O K-edge spectra from 15 nm thick films on LSAT are quite featureless and lack the pre-peak. This has been observed in heavily oxygen deficient perovskites. This fact, together with the shorter modulation length of the vacancy superstructure, suggests that these films contain the most vacancies.

The density of dark stripes observed decreases in the thicker LCO films, indicating that the oxygen vacancy ordering is strain related as previously reported.[15] STEM images in Figure 4 also show that the distribution of vacancy plane orientations is more disordered in these thicker films. Vacancy planes oriented along both IP and OOP directions can be observed in 75 nm films grown on LAO(Figure 4(a)) and STO respectively(Figure 4(c)). Moreover the 75 nm thick film on LSAT(Figure 4(b)) does not show clear evidence of vacancy ordering. Oxygen vacancies often result in expansion of the lattice[22] and may aid in alleviation of tensile stresses in the film from epitaxial strain.[17,18] The periodicity and orientation of the vacancy planes in the thin films (Figure 3) indicate that the vacancies are arranged in the film to relieve the stresses from growth on STO, LSAT, and LAO. Thus vacancies fill the elongated strain directions in the film caused by the lattice mismatch between film and substrate: IP for films on STO and LSAT, OOP for films on LAO. One TEM study[23] on Sr-doped cobaltite films has even cautioned that superstructure can also be the product of TEM beam irradiation which causes deoxygenation

of the sample. We do not believe such a mechanism to be a major issue in our samples, due to the smaller spot size of the STEM beam used and the observations of ordering only under certain sample orientation and thickness conditions. In addition, we do not observe any major average lattice constant enlargements locally in STEM upon irradiation and so it is unlikely that the STEM beam is a major source of deoxygenation. The beam may, however, further order the preexisting oxygen vacancies in the vicinity of the STEM irradiated region.

In addition to the fewer and more disordered dark contrast planes found in these thick samples, thick films on STO also show evidence of film cracking and buckling throughout the film interior(Figure 4(c)). In fact, a similar cracking and buckling has been observed by us at the film surface (using atomic force microscopy) and by other groups in even thicker films on LSAT.[24] This added relaxation mechanism may contribute to the equilibrium stress-strain state in these thicker films and may account for the decreased presence of oxygen vacancy planes in these thicker films.

## III.  ELECTRONIC STRUCTURE

The strain and accompanying defects have a significant effect on the electronic structure, and provide us with the framework to explain the generation of long range magnetic order in our LCO films. In order to probe the electronic structure, we have used XA spectroscopy to
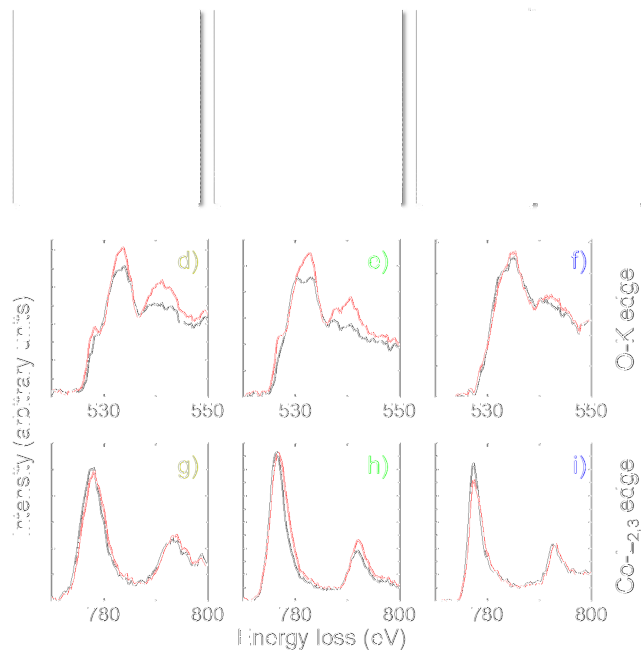
FIG. 3: (color online) Scanning transmission electron microscopy high angle annular dark field images showing periodic dark contrast planes parallel and perpendicular to the substrate-film interface for ~15 nm thick films of $LaCoO_3$ on (a) $LaAlO_3$, (b)$(La,Sr)(Al,Ta)O_3$, and (c) $SrTiO_3$. Co-L edge (g, h, i) and O-K edge (d, e, f) EELS spectra from line scans taken along the bright (red) and dark (black) contrast planes in dark field imaging are shown below the corresponding images.

determine the Co valence distribution in the films. For XA measurements, films were grown on Nb-doped STO (Nb:STO) to prevent the insulating films from charging at low temperatures in total electron yield mode. Measurement of the films on STO, LSAT, and LAO substrates at low temperatures resulted in significant sample charging due to their insulating nature, thus preventing credible analyses of the spectra. At higher temperatures, XA and XLD measurementes were performed for LCO films on STO, LSAT and LAO substrates.

The XA spectra of thin and thick LCO films on Nb:STO substrates reveal the electronic structure changes associated with the epitaxial strain relaxation in the film. Figure 5 shows XA spectra for 15 nm and 70 nm thick films at 25K. The intensities in the figure are the sum of spectra taken under +0.5 T and -0.5 T with circularly polarized X-rays incident at a 30° angle from the sample surface normal. In this geometry (30° grazing incidence), the applied field and X-ray polarization electric field vector have major components oriented along the IP direction of the film. After normalizing the spectra to the peak Co $L_3$ edge intensity (black arrow), spectral differences between the strained (15 nm) and relaxed (70 nm) thick film can be discerned (orange and green arrows). Specifically, the 15 nm film shows a higher intensity ratio of pre-edge shoulder intensity (long orange
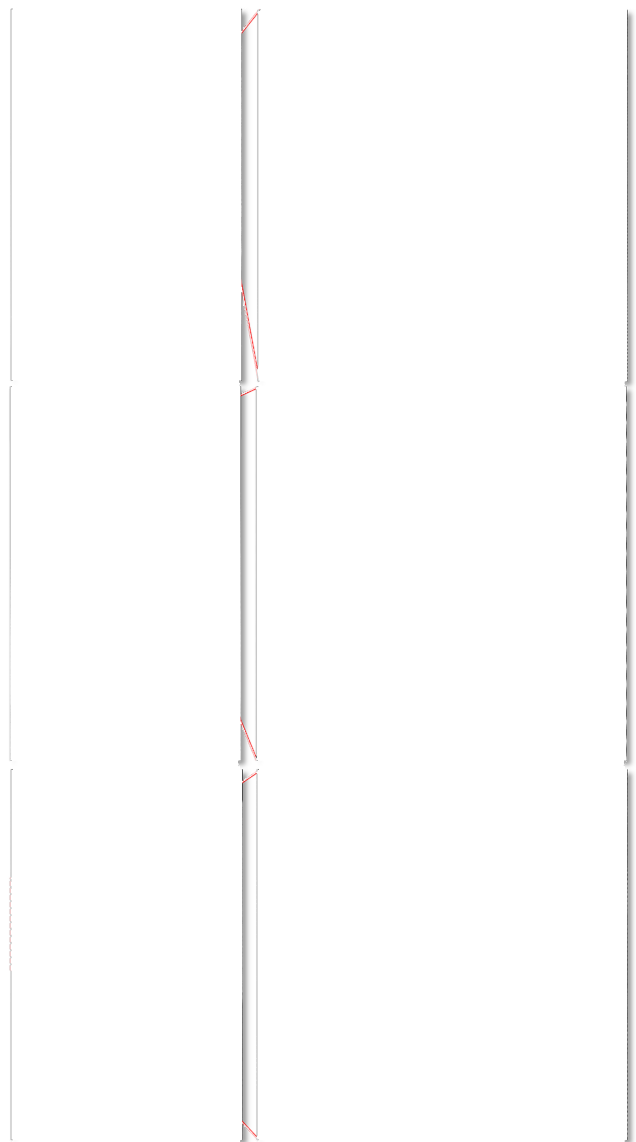


FIG. 4: (color online) Scanning transmission electron microscopy images taken in bright field imaging for 75 nm thick films on (a) LAO, (b) LSAT, and (c) STO.

arrow) to post-edge shoulder intensity (shorter orange arrow) at the $L_3$ peak compared to the 70 nm film. A similar change is also observed in the intensity and ratio of peaks at the $L_2$ edge of the spectra.

In order to interpret the differences in features among the samples in terms of Co valences, we compare the sample spectra to reference spectra of Co in various valences and spin state configurations (Figure 5(b)). The reference spectra serve as effective "fingerprints" of the different spin and valence states in the XA spectra- a common technique used in the analysis of XAS data. The reference spectrum from CoO represents HS $Co^{2+}$ in an octahedral coordination,[25] while $EuCoO_3$ spectrum represents LS $Co^{3+}$ in an octahedral coordination.[26] The
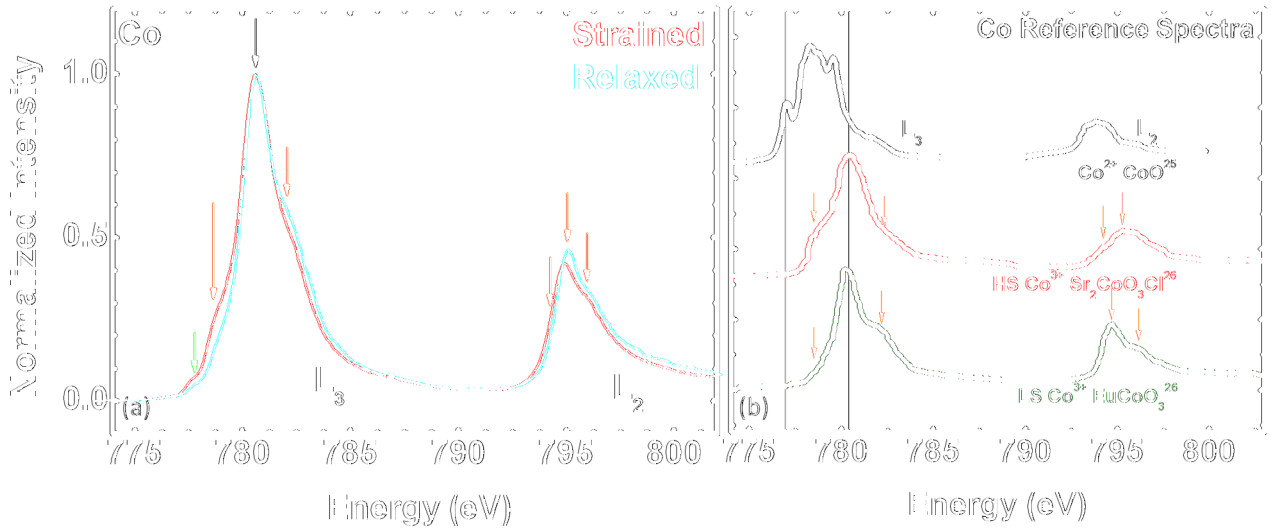
FIG. 5: (color online) (a) XA spectra for films grown 15 nm (red) and 70 nm (blue) thick on Nb-doped STO. Arrows indicate relevant features of the spectrum. (b) A set of reference spectra for HS $Co^{2+}$,[25] HS $Co^{3+}$,[26] and LS $Co^{3+}$[26] are provided to analyze the film spectra.
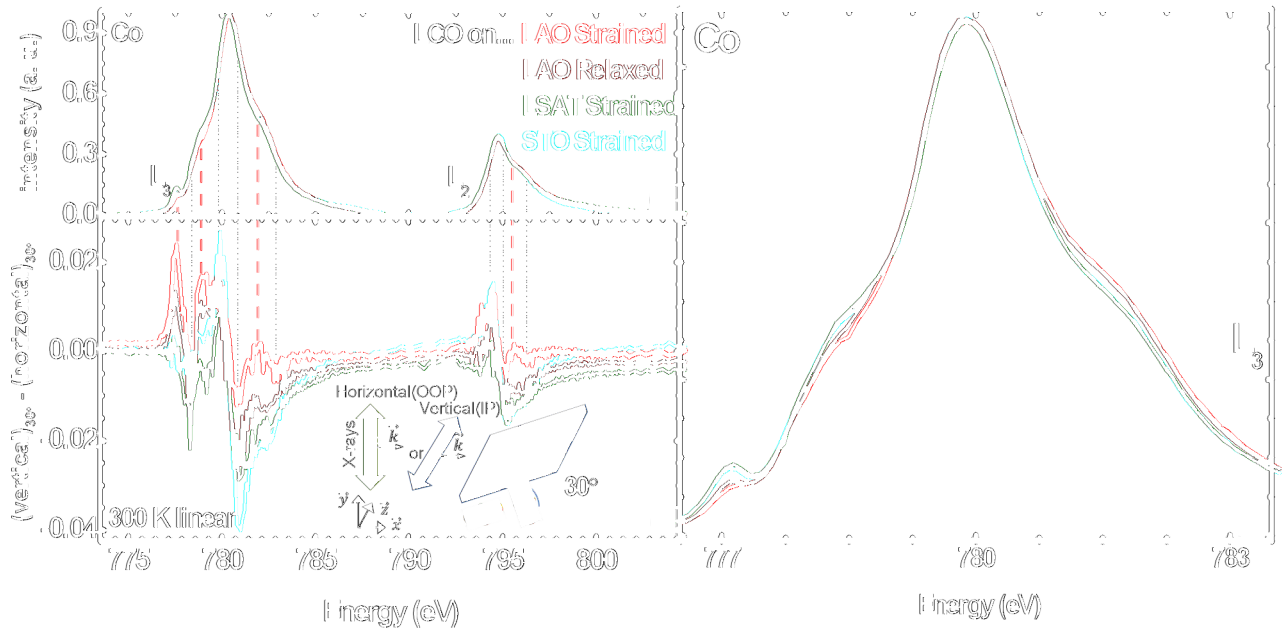


FIG. 6: (color online) (a)XA and XLD (c) for films grown on LAO (red), LSAT (green), and STO (blue). The figure on the right (b) is an enlarged region of the Co - $L_3$ edge showing the differences in spectral features.

only available reference spectra for purely HS $Co^{3+}$ is that of $Sr_2CoO_3Cl$ where HS $Co^{3+}$ is in a pyramidal coordination.[26] This spectrum's lineshape is also similar to the XA spectrum of an octahedrally coordinated $Fe^{2+}$ ($3d^6$) ion which has the same electron configuration as HS $Co^{3+}$.[26] While temperature dependent spectra of octahedrally coordinated Co in a mixture of high and low spin configurations do exist for bulk LCO (and show similar line shape trends with temperature and spin state)[27] we chose these extreme cases (100% HS and 100% LS

at 300K) for our comparisons. But even in these references the differences are subtle and it is difficult to make strong statements concerning the quantity of HS $Co^{3+}$ in our samples. There are features in the $Sr_2CoO_3Cl$ at 778eV and 794eV that may be correlated with those in our samples. In any case, the presence of HS $Co^{3+}$ cannot be ruled out in our samples.

Features at the Co L edge in CoO provide signatures for HS $Co^{2+}$ ions. The pre-edge $L_3$ feature at ~777 eV (green line) in the reference CoO spectrum[25] is not repro-

duced in either of the reference $Co^{3+}$ spectra from Hu *et al.* which suggests that any intensity at this energy can predominantly be associated with some presence of $Co^{2+}$ in the sample.[28] Thus, both the strained and relaxed films of LCO on STO show an indication of some amount of HS $Co^{2+}$ present in the film as suggested by the small intensity shoulder near ~777 eV (Figure 5(a), green arrow). The intensity difference at this energy between the two films indicates that the strained film shows an increased presence of HS $Co^{2+}$ compared to the relaxed LCO film. This result is consistent with the accommodation of strain by the presence of oxygen vacancies in the film.

We also compared the spectra of the 15 nm and 75 nm LCO films on Nb-doped STO with reference LS $Co^{3+}$ spectra from $EuCoO_3$.[26] The reference spectra indicate that LS $Co^{3+}$ has a higher post-edge shoulder intensity at the $L_3$ edge and higher pre-edge shoulder intensity at the $L_2$ edge. In the relaxed LCO film the relative ratios near the $L_3$ and $L_2$ edges are similar to the LS $Co^{3+}$. The strained films show an increased intensity at the pre-edge shoulder feature of the $L_3$ edge and a decreased intensity at the post-edge shoulder feature of the $L_3$ edge, contrary to that of LS $Co^{3+}$. The relative ratio of pre and post edge intensities cannot be explained solely in terms of HS $Co^{2+}$ and LS $Co^{3+}$ when compared to the relevant reference spectra. Thus, when comparing strained and relaxed films grown on Nb-doped STO we conclude that: (i) in both films at least some amount of $Co^{2+}$ exists (strained films may have more), (ii) in relaxed films, we find mostly LS $Co^{3+}$; and (iii) in strained films, LS $Co^{3+}$ and possibly some HS $Co^{3+}$ exists.

Room temperature XLD (i.e. linear dichroism in the absence of a magnetic field) was used to compare differences in electronic occupation of the Co $d$-orbitals for strained films on STO, LSAT, and LAO, and a relaxed film on LAO. By measuring the linear dichroism at room temperature without a magnetic field, we are able to minimize charging effects from the insulating samples, and we ensure that the observed linear dichroism is from bonding anisotropies and not magnetic anisotropy in the film. With the sample at 30° grazing incidence, vertical and horizontal linearly polarized X-rays can be used to probe IP and OOP hole density of the Co ion electron configuration. The difference of the XA spectra from vertically and horizontally polarized X-rays is plotted as the XLD signal.

Figure 6 shows the orientation-averaged XA spectra and corresponding XLD intensity. The XA spectra (Figure 6(a, b)) for films grown on different substrates show subtle intensity differences at the $L_3$ and $L_2$ edges associated with HS $Co^{2+}$, LS $Co^{3+}$, and possibly HS $Co^{3+}$ features discussed previously. In particular, LSAT films have the highest intensity at the pre-edge shoulder associated with HS $Co^{2+}$, followed by STO, relaxed LAO, and, finally, strained LAO. This trend is consistent with findings of increased oxygen vacancies for LSAT films from STEM and EELS studies.

The XLD spectra in Figure 6(c) shows that there is a clear difference in the IP and OOP hole density in the various films due to difference in the epitaxial strain state. Since the relative amount of HS $Co^{2+}$, LS $Co^{3+}$ and HS $Co^{3+}$ in each sample is fixed, the resulting linear dichroism is due to differences in electronic structure along different orientations for one fixed composition. The dashed red lines in Figure 6(c) indicate the most significant differences between the samples. We find the strongest differences between films grown in tension on STO and LSAT and films strained in compression on LAO. Films relaxed on LAO have a linear dichroism spectra that shares some similarities with both strained films on LAO and strained films on LSAT and STO. While many of the dichroism differences may be due to different contributions from HS $Co^{2+}$, LS $Co^{3+}$, and HS $Co^{3+}$[28] in each sample, lattice distortions can also influence the anisotropies in charge density.[29] At the $L_3$ edge, it would be difficult to deconvolve the effects of lattice distortions and different distributions of HS $Co^{2+}$, LS $Co^{3+}$, and HS $Co^{3+}$ in the various XLD spectra. However, near the $L_2$ edge, the linear dichroism from HS $Co^{2+}$, and undistorted LS $Co^{3+}$ ions is known to be negligible.[28] Although we do not have a pure octahedral HS $Co^{3+}$ reference spectrum, HS $Co^{3+}$ in $Sr_2CoO_3Cl$[26] and $Fe^{2+}(3d^6)$[26] both show little contribution to the $L_2$ edge of the linear dichroism data. Thus, the strong linear dichroism feature near the $L_2$ edge in all samples is likely accounted for by a contribution from tetragonal distortion of the LS $Co^{3+}$. Thus, differences in XLD near the $L_2$ edge for the different samples are likely associated with differences in the tetragonal distortion of the LS $Co^{3+}$ ions. Since films grown on LAO have c/a >1 and films grown on LSAT and STO have c/a <1, this additional contribution to the anisotropic charge density is consistent with a distortion of the Co-O octahedral cage under epitaxial strain. Together, XA spectroscopy and XLD indicate that the different quantities of oxygen vacancies and degree of tetragonal lattice distortions in the films affect the anisotropic charge density and the Co ion distribution found in all films.

## IV. MAGNETISM

### A. Bulk Magnetometry

Ferromagnetism is consistently found in films strained in tension. Figure 7 shows the SQUID magnetometry results for films grown ~15 nm thick (labeled as *strained*) and ~75 nm thick (labeled as *relaxed*) on STO, LSAT and LAO substrates measured with the field applied in the film plane. Coherently strained films in tension on LSAT and STO both show evidence of ferromagnetic order. However, it is interesting that 15 nm films on LSAT, which are under smaller strain compared to films on STO, have the highest saturated moment of ~2.15 $\mu_B$/Co (Figure 7(b)). By increasing the tetragonal distortion and epitaxial strain by growth on STO, we find a lower sat-

urated moment of ∼0.85 $\mu_B$/Co (Figure 7(a)). On the other hand, 15 nm thick films strained on LAO do not show ferromagnetic hysteresis (Figure 7(c)), magnetic remanance, or Curie temperature (Figure 7(d)) in any direction, thus suggesting that epitaxial compressive strain does not give rise to ferromagnetism.

In contrast to the 15 nm films, all ∼75 nm thick films (even those on LAO) show ferromagnetic behavior below ∼85 K. However, just as we observed in the trends for 15 nm thick films, even in these 75 nm thick samples, LCO on STO has a lower moment (∼0.6 $\mu_B$/Co) compared to LCO films on LSAT (∼0.95 $\mu_B$/Co). Figure 8(a) shows how the saturated moment on STO decreases as a function of increasing thickness. Surprisingly, while the coherently strained films in compression on LAO did not show any magnetism, relaxation of the epitaxial strain on thicker films resulted in ferromagnetic ordering (Figure 8(b)). In these thicker films, although the strain and tetragonal distortion is presumably much smaller, the ferromagnetic signal is greater. This result suggests that additional factors besides strain need to be considered in explaining all the details of the ferromagnetism.

These results show that films strained in tension clearly result in long-range ferromagnetic order below ∼85 K. The decrease in overall ferromagnetic response in thick films on STO and LSAT is expected due to the structural relaxation towards bulk lattice parameter values. Hence, strain contributes to ferromagnetic order in LCO films. In the 75 nm thick films on STO and LSAT the lower net moment can be attributed to some mixture of relaxed film and film still strained to the substrate as well as possible strain gradients. However, bulk LCO at these temperatures is mostly composed of diamagnetic LS Co, so that the evidence of ferromagnetism in the relaxed films on LAO is surprising. This result suggests that though the lattice parameters in the relaxed LCO film on LAO appear to be similar to bulk LCO, the defects and stoichiometry are not similar and contributes to long-range ferromagnetic order. Also intriguing is the presence of higher moment in coherently strained films grown on LSAT compared to more tensilely strained films grown on STO. If the magnetism were purely strain related, more highly strained films on the larger lattice-mismatched substrate, STO, would have the highest moment. Others have also observed the ferromagnetic signal from LCO/LSAT samples to be more than that from LCO/STO samples.[5,14] Since LSAT has the highest magnetic moment, additional sources must also contribute to the magnetism.

### B. X-ray Magnetic Circular Dichroism

Having established the presence of Co ions in various spin states via XA spectra, we now directly correlate the presence of these Co spin states with the ferromagnetism using XMCD. This technique probes the spectral changes associated with the changes in applied magnetic field.

Thus, we can qualitatively assess the role of these constituent Co ions in the magnetic response. Figure 9 shows the XMCD at 25 K from an 8 nm strained film and a 75 nm relaxed film grown on Nb-doped STO measured below the magnetic ordering temperature of 75-80K. Overall, the presence of XMCD signal in this geometry is consistent with the presence of in-plane magnetization measured in SQUID magnetometry. The largest dichroism intensity appears near the peak labeled (b) in the corresponding XA spectrum. The small HS $Co^{2+}$ feature at 777 eV and near the shoulder labeled (a) does indicate a contribution to the magnetic dichroism intensity from HS $Co^{2+}$ ions. This signal appears in addition to the larger XMCD signal at the peak labeled (b) in the strained LCO films on STO. Comparison with XMCD reference spectra for HS $Co^{2+}$ from Figure5(b) suggests that the peak at (b) cannot be explained in terms of HS $Co^{2+}$. It is also worth mentioning that we expect the LS $Co^{3+}$ to contribute no moment (since S=0), thus suggesting that the largest contribution to the XMCD signal is from HS $Co^{3+}$. Finally we find that the corresponding feature at the peak labeled (c) in the XMCD is not as prominent as in the XAS. In the 75 nm film, the dichroism intensity is lower compared to the 8 nm film, consistent with the finding that the net moment per Co ion from the 75 nm film is lower than that of the 8 nm film from SQUID magnetometry. Since the XA measurement is highly surface sensitive, the lower net moment measured from SQUID magnetometry cannot be associated with a few strained layers closest to the substrate-film interface, but must arise from (partially relaxed) layers at the surface of the film as well.

## V. DISCUSSION

In our comprehensive study of epitaxial LCO films on STO, LSAT and LAO substrates, we show that that the ferromagnetism hinges on two key effects: tensile epitaxial strain and oxygen vacancies. Tensile epitaxial strain is crucial for the stabilization of HS Co ions but the long range ferromagnetic order also is greatly enhanced by oxygen vacancy defects. Previous work has shown that ferromagnetic moment is highest in films strained in tension.[5,6,10] In LCO films, Merz et al. have explained the observation of ferromagnetism in terms of a superexchange interaction among LS and HS $Co^{3+}$ ions mediated by a correlated hopping.[3] Our own previous work on $PrCoO_3$ films has also shown the importance of the HS $Co^{3+}$ ions in the exchange mechanism that gives rise to the insulating long-range ferromagnetic order in the Co sublattice.[30] In addition to this spin configuration fluctuation model, our recent first principle calculations that incorporate epitaxial strain and ordered oxygen vacancy effects explain the ferromagnetic response of oxygen deficient epitaxial $LaCoO_3$ thin films on STO substrates.[4] That work explored thin films on STO and showed modeling which explained how a small number of oxygen va-
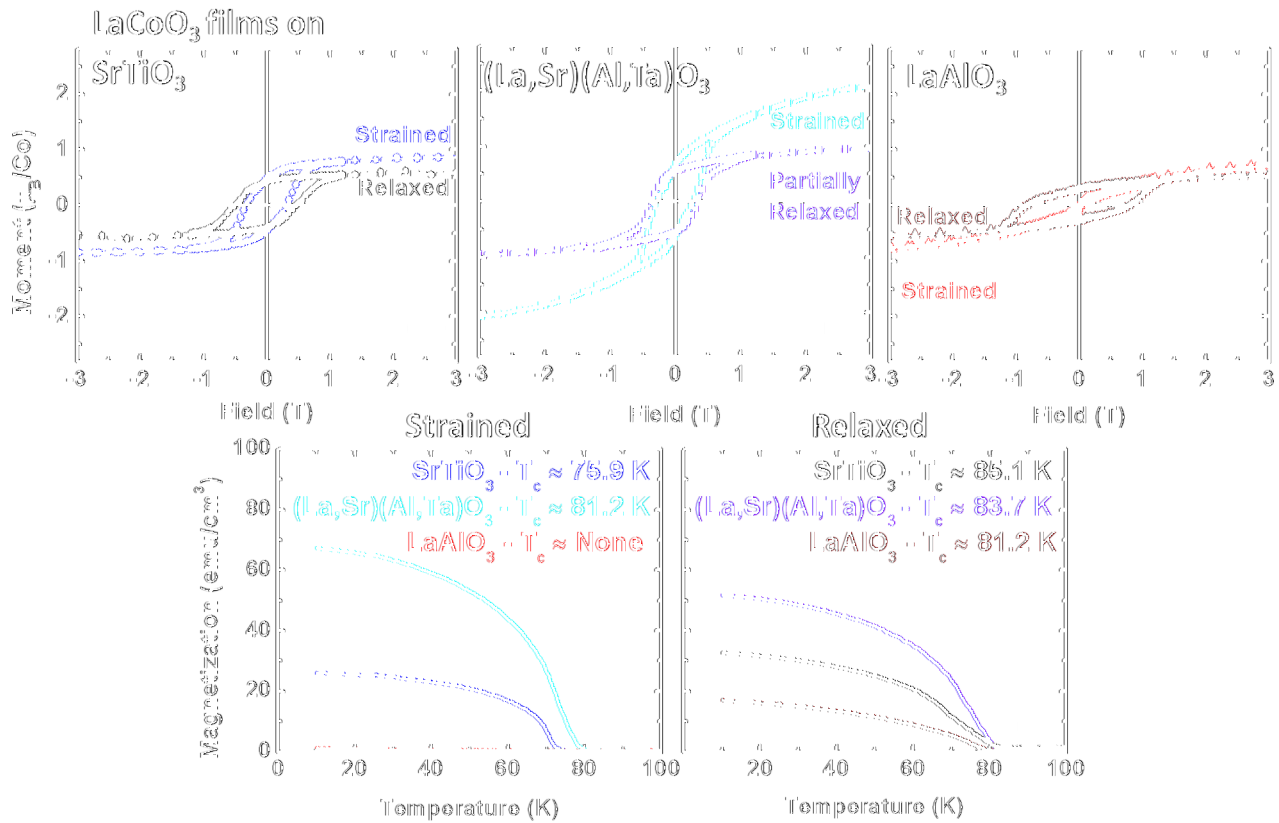
FIG. 7: (color online) Magnetization vs field measurements at 5 K for thin (dark) and thick (light) LCO films grown on (a) STO, (b) LSAT, and (c) LAO substrates showing a range of saturated moments. The magnetization vs temperature measurements under H=5 mT (FC) for (d) strained and (e) relaxed films show a Curie temperature below ∼85 K for all films except strained films on LAO.

cancies on the order ≤11% could give rise to a ferromagnetic order via a mixture of antiferromagnetic and ferromagnetic tetrahedral HS $Co^{2+}$ and $Co^{3+}$. Therefore both superexchange interactions among HS $Co^{3+}$ and LS $Co^{3+}$ ions mediated by correlated hopping as well as superexchange interactions among HS $Co^{2+}$ and LS $Co^{3+}$ ions likely contribute to the observed long range magnetic order in our LCO films.

The presence of ferromagnetism in tensilely strained LCO films, and not in compressively strained films less than 15 nm thick, indicates that epitaxial strain plays some role in stabilizing ferromagnetism. However, the presence of defects observed by STEM and EELS associated with growth on different substrates suggests that the role of the microstructure must also be taken into consideration. The STEM images show that in 15 nm thick films there are a large number of oxygen vacancies and likely a considerable number of $Co^{2+}$ ions distributed throughout the films. The magnitude and ordering of these oxygen vacancies is related to the sign and magnitude of the substrate-induced strain in the films and may also affect the magnetic ordering. For example, 15 nm tensilely strained films on LSAT which have the highest magnetic moment show the most defects, as indicated by

their occurrence every 2-3 unit cells perpendicular to the film plane. 15 nm films on STO are also strained in tension but have slightly fewer oxygen defect planes (every 3-4 unit cells perpendicular to the film plane) and have a lower moment compared to films on LSAT. Finally, 15 nm films on LAO are strained in compression, have even fewer oxygen defect planes occurring along the film plane every 3-4 unit cells and do not show any long-range ferromagnetic order. These results suggest that the number of oxygen defects, the orientation of the defect planes, the strain state all play a role in the generation of long range ferromagnetic order.

The ferromagnetic moment appears to be positively correlated with the quantity of oxygen vacancies and negatively correlated with film thickness for films in compression and tension. For example, while in 15 nm films on LAO only defect planes parallel to the substrate-film interface are observed, in 75 nm films the planes appear both parallel and perpendicular to this interface, suggesting an overall increase in the total number of defects and a relaxation of the compressive strain state. The increased magnetism in thicker LAO film, suggests that there is a connection between magnetism and the greater number of defects oriented perpendicular to the
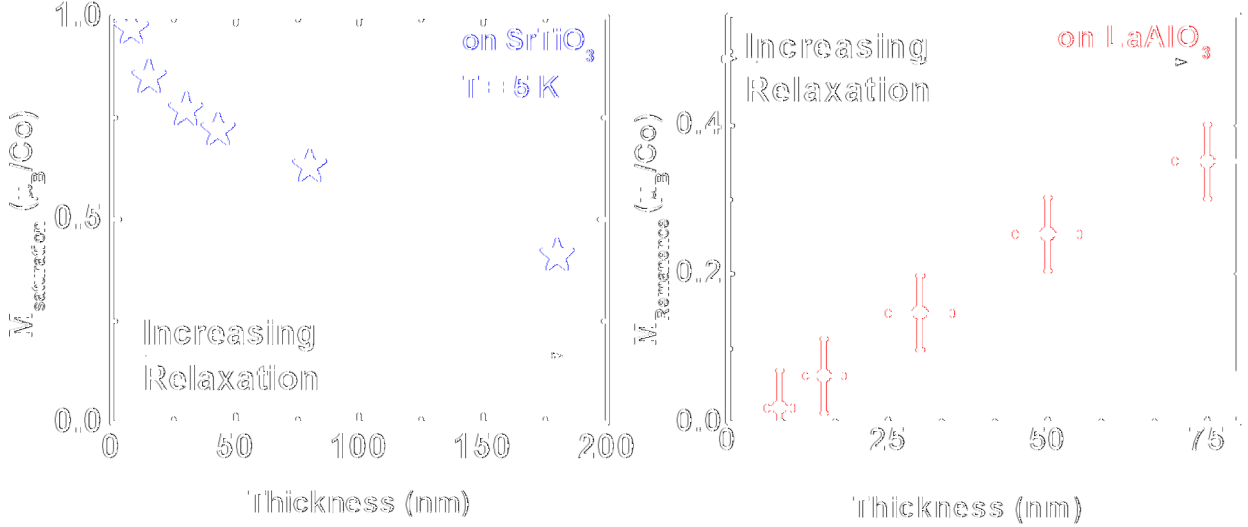
FIG. 8: (color online) Magnetism trends as a function of increasing film thickness and hence relaxation showing that films on (a) STO exhibit a decreasing saturated moment and films on (b) LAO exhibit an increasing remanent moment.
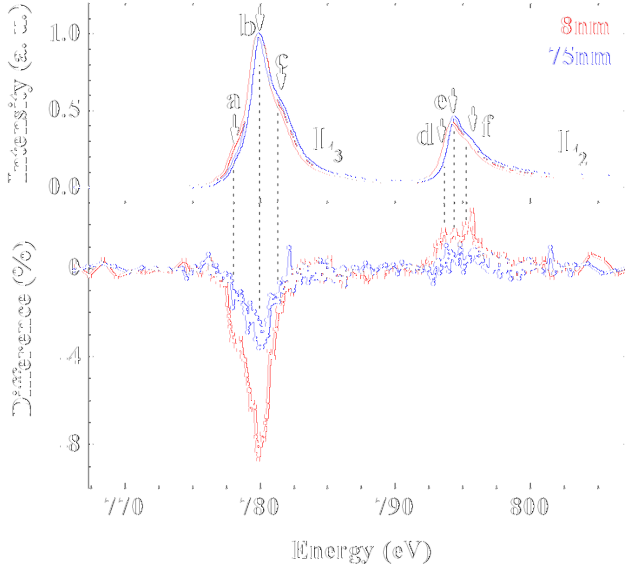


FIG. 9: (color online) XA (top panel) and corresponding XMCD (bottom panel) spectra for 8 nm and 75 nm films grown on Nb-doped STO measured at 25K using circularly polarized X-rays in an alternating 1.5 T magnetic field applied 30 degrees from the in-plane direction.

film plane. In thicker films on LSAT and STO, there is a decrease in defect planes perpendicular to the film plane, a net decrease in the number of defects, and a relaxation of the tensile strain state in the film. If the parameters of strain and defects both play a role in the magnetism then these changes are consistent with the increased moment in thicker films on LAO and the decreased moment

in thicker films on STO and LSAT. The lack of obvious defects in the thick ferromagnetic film on LSAT indicates that the defects may not always be necessary to stabilize long-range ferromagnetic order, though their presence enhances it, as observed in the 15 nm films.

Together the stoichiometric, structural, and magnetic trends of LCO films from the data allows us to construct a qualitative picture of the exchange mechanisms that may be responsible for the ferromagnetism observed in these LCO films. The picture must explain a number of experimental observations. (1) Films strained with expanded IP lattice parameters have a moment of $\sim 2$ $\mu_B$/Co on LSAT and $\sim 1$ $\mu_B$/Co on STO. Films strained with contracted IP lattice parameters do not show long-range magnetic order. (2) The highest moment we observe (strained LCO films on LSAT) is associated with the greatest number of oxygen vacancy planes (every 2-3 unit cell perpendicular to the film plane). Nonmagnetic films (on LAO) are associated with few oxygen vacancy ordering planes (every 3 unit cells oriented parallel to the film plane). (3) Despite the variations in saturated moment, all magnetic films are insulating and have a Curie temperature <85 K.

Our work suggests that a new model is necessary to explain both the role of vacancies and epitaxial strain in stabilizing long-range ferromagnetic order in this system. On the one hand, ferromagnetism in epitaxial LCO films has been attributed to a superexchange interaction among LS and HS $Co^{3+}$ ions mediated by a correlated hopping. We do see evidence for the presence of HS $Co^{3+}$ in our XMCD data (Figure 9) along with the presence of LS $Co^{3+}$ in the XA data. Thus, correlated hopping cannot be ruled out in our samples. On the other hand, through previous density functional theory modeling[4] we found that a checkerboard array of HS $Co^{2+}$ combined
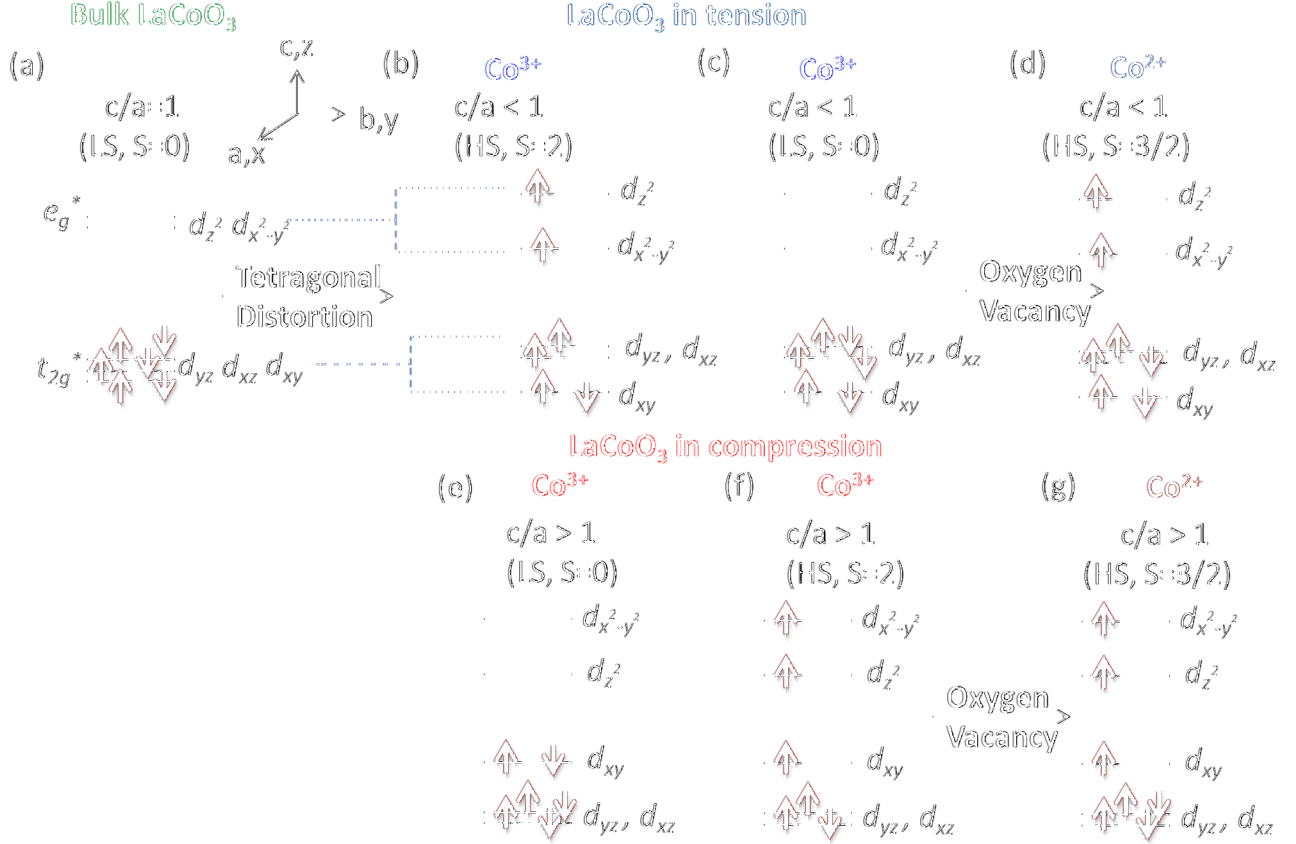
FIG. 10: (color online) Schematic electron configurations associated with growth on STO and LSAT substrates showing (a) bulk LS $Co^{3+}$, (b) tetragonally-distorted HS $Co^{3+}$, (c) tetragonally-distorted LS $Co^{3+}$, and (c) tetragonally-distorted, oxygen-deficient HS $Co^{2+}$. Also shown are the configurations for LCO on LAO substrates showing (e) tetragonally-distorted LS $Co^{3+}$, (f) tetragonally-distorted HS $Co^{3+}$, and (g) tetragonally-distorted, oxygen-deficient HS $Co^{2+}$.

with LS $Co^{3+}$ may give rise to ferromagnetic ordering as well. For this model to apply we need only oxygen vacancy ordering at short length scales; this is consistent with the XRD data that do not show evidence for coherent long range ordering of the oxygen vacancies while STEM data show evidence for short range oxygen vacancy ordering. Furthermore, our XMCD data suggests that there is some contribution from HS $Co^{2+}$ in our samples. Indeed, we cannot fully rule out either of these two mechanisms. Since our results suggest that in fact both of these mechanisms play some role depending on the sample being studied, we present a framework to describe the possible pathways due to symmetry that may give rise to an insulating ferromagnetic exchange in this system.

Figure 10 shows a set of qualitative electron configuration models based on some likely effects of the lattice distortions and oxygen vacancies on the Co energy levels. The figures show schematic representations for: unstrained pseudocubic LCO in a LS state; HS $Co^{3+}$ under a strain-induced tetragonal distortion; LS $Co^{3+}$ under a strain-induced tetragonal distortion; and HS $Co^{2+}$

also in a tetragonally-distorted octahedral crystal field. This does not include all possible spin and valence state configurations possible for the Co ion under these strain conditions, but addresses the most likely electronic configurations suggested from our results. These electronic configurations provide the framework for possible local ferromagnetic exchange interactions among different Co spin and valence states in the films. These diagrams neglect the fact that in an extended crystal with a mixture of ionic and covalent bonding, these energy levels would be better visualized as electron bands than discrete isolated energy levels. We have assumed a pseudocubic octahedral ligand field where the Co-O molecular orbitals are split into the three-fold degenerate nonbonding $t_{2g}$ and two-fold degenerate antibonding $e_g$* shells. For simplicity, in the HS and LS schematics, the exchange-split spin-up and spin-down levels have been drawn on a redundant energy scale for all $e_g$* and $t_{2g}$ orbitals, while in a more accurate depiction we might expect the minority-spin (spin-down) electron levels in HS states to be higher in energy than the majority-spin (spin-up) $e_g$* levels.

Figure 10(a) shows the electronic configuration for

undistorted bulk-like LS Co$^{3+}$ in pseudocubic LCO which has no net spin moment (S=0) and behaves as a diamagnetic insulator at low temperatures in the bulk. Figure 10(b-d) show the schematic change in symmetry of the LCO unit cell due to presumed bond-length distortions induced by epitaxial tensile strain. As a result of the decreased $z$-axis length and increased $x,y$-axis length, the $e_g$* and $t_{2g}$ orbital degeneracy is further reduced and the octahedral $O_h$ symmetry is reduced to $D_{4h}$ symmetry. The anti-bonding and non-bonding molecular orbitals, which have mostly transition metal-like $d$-orbital character, shift in relative energy position. Due to the presumed bond length distortions from the epitaxial strain, $d$-orbitals with $x,y$-axis components have decreased overlap with neighboring oxygen orbitals. The decreased overlap results in a relative decrease in energy of these antibonding and nonbonding molecular orbitals. Another electron configuration possibility introduced in these investigations is the HS Co$^{2+}$ ion, which may be present due to the observed oxygen vacancies in the film (Figure 10(d)). XLD suggests that a distorted lattice from epitaxial growth is also likely to be found for the Co$^{2+}$ ions. The electron configuration for Co$^{2+}$ in a HS state is very similar to HS spin Co$^{3+}$ with one more electron in the $t_{2g}$ sub-band.

A model that explains the ferromagnetic exchange interaction in this mixed spin/mixed valence system must also account for the absence of a ferromagnetic moment in strained films on LAO. Figure 10(e-g) shows the set of possible Co spin and valence states for tetragonally-distorted films of LCO on LAO. The key difference between these electronic structure configurations and the ones for films on LSAT and STO is the relative shift in energy of the different $d$-orbitals due to the different sign of lattice strain. In films on LAO the pure IP orbitals $d_{xy}$ and $d_{x2-y2}$ orbitals are higher in energy due to the shorter IP bond lengths. This change would cause only a subtle difference in the $e_g$* electron filling between the films on LAO and films on LSAT and STO. However, in the $t_{2g}$ orbitals this results in a lower energy for the degenerate set of orbitals, the $d_{xz}$ and $d_{yz}$ orbitals, compared to films on LSAT and STO. This could account for some differences in magnetic behavior, since the holes in the $t_{2g}$ shell in the film on LAO occupy the non-degenerate $d_{xy}$ level, while in contrast the holes in films on LSAT and STO exist exclusively in the degenerate $t_{2g}$ subband. This contrast in hole density between thin ferromagnetic films on LSAT and STO and thin strained non-ferromagnetic films on LAO is consistent with our XLD measurements shown in Figure 6.

The ferromagnetic exchange interaction in the films on LSAT couples a mixture of HS Co$^{3+}$ (S=2, ∼4 $\mu_B$/Co), LS Co$^{3+}$ (S=0, ∼0 $\mu_B$/Co), and HS Co$^{2+}$ (S=3/2, ∼3 $\mu_B$/Co) to result in a net moment in the film of ∼2 $\mu_B$/Co. Films on STO show ferromagnetism most likely through a similar exchange mechanism, but in the case of STO the net moment is only ∼1 $\mu_B$/Co. STEM and EELS have shown that the oxygen vacancy contents of these LSAT and STO films are different, most likely due to the changes in strain and lattice distortions between these two films. The lower moment and decreased oxygen vacancy content of films on STO (compared to films on LSAT) suggest an increased presence of LS Co$^{3+}$ and a corresponding decreased presence of high moment Co$^{2+}$ ions. In a similar way, films grown on LAO also contain a distribution of Co ions that differs from films on STO and LSAT as revealed by the XA spectra and STEM and EELS measurements. In strained films on LAO, the exchange is suppressed among the different Co ions and long-range magnetic ordering does not occur. It is still unclear whether the suppression of long-range order is fully explained by this different mixture of Co ions or through some other means such as the lattice distortions felt by these ions. However, in thicker more relaxed films on LAO, the mixture, distortion, and organization of Co ions in the film changes to allow for long-range ordering to occur.

Until we can accurately measure oxygen content and oxygen-related effects, the role of these defects in correlated electron systems will always be uncertain. The greater underlying challenge is to develop a picture that can account for (i) the presence of long-range ferromagnetism with a robust T$_c$, (ii) a variable saturated moment, and (iii) insulating behavior in LCO films. This will require considerably more work from both theoretical[4,31–34] and experimental perspectives. In our recent STEM investigation[4] for the specific case of LCO films on STO, both the magnitude of the moment and the insulating behavior are accounted for with model calculations explicitly considering the *ordering* of oxygen vacancies in the film. The net moment of ∼1 $\mu_B$/Co for films on STO is accounted for in this previous work with a density functional theory model.[4] In this present study we grew films on all three substrates and find the ordering of oxygen vacancies in planes perpendicular to the sample plane combined with the presence of HS Co ions to stabilize a ferromagnetic ground state in epitaxial LCO films.

In conclusion, LCO is a fascinating system for epitaxial studies due to the delicate balance between crystal field and Hund's energy that is easily perturbed through external parameters. In this work we have demonstrated the important role that epitaxial strain and oxygen vacancies play in determining the ground state of epitaxial LCO thin films. Oxygen vacancies order according to the direction and magnitude of the strain induced by the substrate. Co valence and spin state are affected by substrate choice. The presence of HS Co$^{3+}$ and Co$^{2+}$, in addition to LS Co$^{3+}$, in different proportions depending on the substrate suggest that a combination of superexchange interactions based on correlated hopping among HS and LS Co$^{3+}$[5] and exchange interactions among HS Co$^{2+}$ and LS Co$^{3+}$ in the presence of oxygen vacancies[9,10] is likely responsible for the observed ferromagnetic ground states. More specifically, strained films on LAO do not show FM, while strained films on LSAT

and STO and relaxed films on all three substrates provide the proper combination of strain and oxygen defects that give rise to a mixture of spin and valence states which support long range FM order. These results indicate the importance of strain, defects, and the interdependence of both in understanding the origin of FM.

[1] P. M. Racah and J. B. Goodenough, Phys. Rev. **155**,932 (1967)

[2] J.-Q. Yan, J.-S. Zhou, and J. B. Goodenough, Phys. Rev. B **70**, 014402 (2004)

[3] M. Merz, P. Nagel, C. Pinta, A. Samartsev, H. v. Lohneysen, M. Wissinger, S. Uebe, A. Assmann, D. Fuchs, and S. Schuppler, Phys. Rev. B **82**, 174416 (2010)

[4] N. Biskup, J. Salafranca, V. Mehta, M. P. Oxley, Y. Suzuki, S. J. Pennycook, S. T. Pantelides, and M. Varela, Phys. Rev. Lett. **112**, 087202, (2014)

[5] D. Fuchs, E. Arac, C. Pinta, S. Schuppler, R. Schneider, and H. v. Loehneysen, Phys. Rev. B **77**, 014434 (2008)

[6] A. D. Rata, A. Herklotz, L. Schultz, and K. Dorr, The Eur. Phys. J. B **76**, 215 (2010)

[7] A. Herklotz, A. D. Rata, L. Schultz, and K. Dorr, Phys. Rev. B **79**, 092409 (2009)

[8] V. Mehta and Y. Suzuki, J. Appl. Phys. **109**, 07D717 (2011)

[9] S. Park, P. Ryan, E. Karapetrova, J. W. Kim, J. X. Ma, J. Shi, J. W. Freeland, and W. Wu, Appl. Phys. Lett. **95**, 072508 (2009)

[10] J. W. Freeland, J. X. Ma, and J. Shi, Appl. Phys. Lett. **93**, 212501 (2008)

[11] R. Zhao, K. Jin, Z. Xu, H. Guo, L. Wang, Appl. Phys. Lett. **102**, 122402 (2013)

[12] J. S. White, M. Bator, Y. Hu, H. Luetkens, J. Stahn, S. Capelli, S. Das, M. Dobeli, Th. Lippert, V. K. Malik, J. Martynczuk, A. Wokaun, M. Kenzelmann, Ch. Niedermayer, and C. W. Schneider Phys. Rev. Lett. **111**, 037201 (2013)

[13] Y.-M. Kim, J. He, M. D. Biegalski, H. Ambaye, V. Lauter, H. M. Christen, S. T. Pantelides, S. J. Pennycook, S. V. Khalinin, and A. Y. Borisevich, Nat. Mat. **11**, 888 (2012)

[14] W. S. Choi, J.-H. Kwon, H. Jeen, J. E. Hamann-Borrero, A. Radi, S. Macke, R. Sutarto, F. He, G. A. Sawatzky, V. Hinkov, M. Kim, H. N. Lee, Nano Lett. **12**, 4966, (2012)

[15] J. Gazquez, S. Bose, M. Sharma, M. A. Torija, S. J. Pennycook, C. Leighton, and M. Varela, Appl. Phys. Lett. Mat. **1**, 012105 (2013)

[16] M. A. Torija, M. Sharma, M. R. Fitzsimmons, M. Varela, and C. Leighton, J. Appl. Phys. **104**, 023901 (2008)

[17] S. Stemmer, A. J. Jacobson, X. Chen, and A. Ignatiev, J. Appl. Phys. **90**, 3319 (2001)

[18] D. O. Klenov, W. Donner, B. Foran, and S. Stemmer, Appl. Phys. Lett. **82**, 3427 (2003)

[19] R. Caciuffo, D. Rinaldi, G. Barucca, J. Mira, J. Rivas, M. A. Senaris-Rodriguez, P. G. Radaelli, D. Fiorani, J. B. Goodenough, Phys. Rev. B **59**, 1068 (1999)

[20] P. E. Vullum, R. Holmestad, H. L. Lein, J. Mastin, M.-A. Einarsrud, and T. Grande, Advanced Materials **19**, 4399 (2007)

[21] P. E. Vullum, H. L. Lein, M.-A. Einarsrud, T. Grande, and R. Holmestad, Phil. Mag. **88**, 1187 (2008).

[22] J. P. Buban, H. Iddir, and S. Ogut, Phys. Rev. B **69**, 180102 (2004)

[23] S. G. Ghonge, E. Goo, R. Ramesh, T. Sands, and V. G. Keramidas, App. Phys. Lett. **63** 1628 (1993)

[24] D. Fuchs, L. Dieterle, E. Arac, R. Eder, P. Adelmann, V. Eyert, T. Kopp, R. Schneider, D. Gerthsen, and H. v. Loehneysen, Phys. Rev. B **79**, 024424 (2009)

[25] T. Burnus, Z. Hu, M. W. Haverkort, J. C. Cezar, D. Flahaut, V. Hardy, A. Maignan, N. B. Brookes, A. Tanaka, H. H. Hsieh, H.-J. Lin, C. T. Chen, and L. H. Tjeng, Phys. Rev. B **74**, 245111 (2006)

[26] Z. Hu, H. Wu, M. W. Haverkort, H. H. Hsieh, H. J. Lin, T. Lorenz, J. Baier, A. Reichl, I. Bonn, C. Felser, A. Tanaka, C. T. Chen, and L. H. Tjeng, Phys. Rev. Lett. **92**, 207402 (2004)

[27] M. W. Haverkort, Z. Hu, J. C. Cezar, T. Burnus, H. Hartmann, M. Reuther, C. Zobel, T. Lorenz, A. Tanaka, N. B. Brookes, H. H. Hsieh, H. -J. Lin, C. T. Chen, and L. H. Tjeng, Phys. Rev. Lett. **97**, 176405 (2006)

[28] C. F. Chang, Z. Hu, H. Wu, T. Burnus, N. Hollmann, M. Benomar, T. Lorenz, A. Tanaka, H.-J. Lin, H. H. Hsieh, C. T. Chen, and L. H. Tjeng, Phys. Rev. Lett. **102**, 116401 (2009)

[29] S. I. Csiszar, M. W. Haverkort, Z. Hu, A. Tanaka, H. H. Hsieh, H.-J. Lin, C. T. Chen, T. Hibma, and L. H. Tjeng, Phys. Rev. Lett. **95**, 187205 (2005)

[30] V. V. Mehta, S. Bose, J. M. Iwata-Harms, E. Arenholz, C. Leighton, and Y. Suzuki, Phys. Rev. B **87**, 020405 (2013)

[31] K. Gupta and P. Mahadevan, Phys. Rev. B **79**, 020406 (2009)

[32] J. M. Rondinelli and N. A. Spaldin, Phys. Rev. B **79**, 054409 (2009)

[33] H. Hsu, P. Blaha, and R. M. Wentzcovitch, Phys. Rev. B **85**, 140404 (2012)

[34] H. Seo, A. Posadas, and A. A. Demkov, Phys. Rev. B **86**, 014430 (2012)